PREPRINT of an article accepted for JARO, August 6, 2008. DOI: 10.1007/s10162-008-0137-8

Sparc Protein Is Required for Normal Growth of Zebrafish Otoliths

YOUNG-JIN KANG[1,2,3], AMY K. STEVENSON[1,2], PETER M. YAU[4,5], AND RICHARD KOLLMAR[1,2,3]

[1]*Department of Molecular and Integrative Physiology, University of Illinois at Urbana-Champaign, Urbana, IL 61801, USA*
[2]*Beckman Institute for Advanced Science and Technology, University of Illinois at Urbana-Champaign, Urbana, IL 61801, USA*
[3]*Neuroscience Graduate Program, University of Illinois at Urbana-Champaign, Urbana, IL 61801, USA*
[4]*Roy J. Carver Biotechnology Center, University of Illinois at Urbana-Champaign, Urbana, IL 61801, USA*
[5]*Department of Cell and Developmental Biology, University of Illinois at Urbana-Champaign, Urbana 61801, IL, USA*

Short Title: Sparc and Otolith Growth

Correspondence to: Richard Kollmar · Department of Molecular and Integrative Physiology · University of Illinois at Urbana-Champaign · 407 South Goodwin Avenue, MC-114, Urbana, IL 61801, USA. Telephone +1-217-333-9861; fax: +1-217-333-1133; email rkollmar@uiuc.edu

Abstract

Otoliths and the homologous otoconia in the inner ear are essential for balance. Their morphogenesis is less understood than that of other biominerals, such as bone, and only a small number of their constituent proteins have been characterized. As a novel approach to identify unknown otolith proteins, we employed shotgun proteomics to analyze crude extracts from trout and catfish otoliths. We found three proteins that had not been associated previously with otolith or otoconia formation: 'Secreted acidic cysteine rich glycoprotein' (Sparc), an important bone protein that binds collagen and Ca^{2+}; precerebellin-like protein, which contains a C1q domain and may associate with the collagenous otolin-1 during its assembly into a framework; and neuroserpin, a serine protease inhibitor that may regulate local protease activity during framework assembly. We then used the zebrafish to investigate whether Sparc plays a role in otolith morphogenesis. Immunodetection demonstrated that Sparc is a true constituent of otoliths. Knockdown of Sparc expression in morphant zebrafish resulted in four principal types of defective otoliths: smaller, extra and ectopic, missing and fused, or completely absent. Smaller size was the predominant phenotype and independent of the severity of otic-vesicle defects. These results suggested that Sparc is directly required for normal otolith growth.

Keywords: inner ear, morphogenesis, biomineral, proteomics, immunofluorescence, antisense oligonucleotides

Introduction

Otoliths ("ear stones") and the homologous otoconia ("ear dust") are essential to the sense of balance; they convey linear accelerations, including gravity, to sensory hair cells in the inner ear (Hudspeth 1989). Their loss or dislocation causes various forms of disequilibrium, including benign paroxysmal positional vertigo, the most common balance disorder in humans (Brandt 2001). The ear of actinopterygii (ray-finned fishes) contains only three large otoliths–the lapillus in the utricle, the sagitta in the saccule, and the asteriscus in the lagena–each with a distinctive and species-specific shape (Nolf 1985). In contrast, the vestibular organs of sarcopterygii (lobe-finned fishes or higher vertebrates) hold innumerable small and barrel-shaped otoconia. Otoconial growth is completed during early postnatal stages, whereas otoliths continue to grow throughout life under the influence of circadian and seasonal rhythms; the resulting growth rings form a stable record of a fish's life history (Campana and Thorrold 2001).

Despite their intriguing shapes and physiological importance, little is known about the formation of otoliths and otoconia (Söllner and Nicolson 2004; Hughes et al. 2006). Unlike bone, they consist of microcrystalline calcium carbonate, rather than phosphate, and are completely acellular. The key regulators of their morphogenesis are therefore thought to be the constituent proteins, which account for less than 5% of their weight. In analogy to other biominerals (Weiner and Addadi 1997), large and insoluble "framework" proteins may form a matrix that determines the site of morphogenesis, whereas small and highly charged "control" proteins may direct the deposition of Ca^{2+} and CO_3^{2-} ions and thus determine the otolith's or otoconium's shape.

Many proteins in otoliths and otoconia remain unknown (Lundberg et al. 2006). Each complement amounts to up to two dozen different proteins, as determined by gel electrophoresis (Pote et al. 1993; Wang et al. 1998 ; Verpy et al. 1999; Murayama et al. 2000; Murayama et al.

2002; this manuscript). Only five proteins have been located in otoliths or otoconia as well as functionally characterized. First, otoconin 90, the major otoconia protein, in mouse (Wang et al. 1998; Verpy et al. 1999; Zhao et al. 2007) and zebrafish (Petko et al. 2008), and its homolog otoconin 22 in frog (Pote et al. 1993; Yaoi et al. 2004). Second, otolith matrix protein-1, the major otolith protein, in trout and zebrafish (Murayama et al. 2000; Murayama et al. 2004; Murayama et al. 2005). Third, otolin-1, a collagenous protein, in salmon and zebrafish (Murayama et al. 2002; Murayama et al. 2004; Murayama et al. 2005) and in mouse (Zhao et al. 2007). Fourth, starmaker, a member of the secretory calcium-binding phosphoprotein family, in zebrafish (Söllner et al. 2003) and otolith matrix macromolecule-64, its likely ortholog, in trout (Tohse et al. 2008). Fifth, secreted phosphoprotein 1 or osteopontin, a secretory calcium-binding phosphoprotein prominent in bone and dentin, in mouse (Sakagami 2000; Thalmann et al. 2006; Zhao et al. 2008). Another half dozen proteins, including calbindin D-28K (Piscopo et al. 2003; Piscopo et al. 2004), SPARC-like 1, countertrypin, and fetuin-A (Thalmann et al. 2006; Zhao et al. 2007), have been only located in otoconia, but not yet characterized.

To identify and characterize novel otolith proteins, we have combined the use of trout and catfish as rich sources for proteomics and of zebrafish as a tractable model for functional studies. Here, we report 'secreted acidic cysteine rich glycoprotein' (Sparc; also known as osteonectin or BM-40), precerebellin-like protein (Cblnl), and neuroserpin (SerpinI1) as constituent otolith proteins. Furthermore, we demonstrate that Sparc, a major bone protein, is required for normal otolith growth. All three proteins may interact with otolin-1 during the assembly of the otolith framework and mineralization.

Materials and methods

Animal husbandry

All experiments were conducted in accordance with a protocol approved by the University of Illinois Institutional Animal Care and Use Committee. Zebrafish (Scientific Hatcheries, Huntington Beach, CA) were maintained live under standard conditions (Westerfield 2000) and staged according to Kimmel and colleagues (1995).

Otoliths

Adult fish heads were from the following sources: white sturgeon, Stolt Sea Farm, Elverta, CA; bighead carp, Big River Fish Corp., Pearl, IL; channel catfish, USDA ARS Catfish Genetics Research Unit, Stoneville, MS, and Illinois Fish Farmers Cooperative, Pinckneyville, IL; black ghost, Dr. Mark Nelson, University of Illinois, Urbana, IL; rainbow trout, Idaho Trout Co., Buhl, ID or Schnucks, Urbana, IL; and tilapia, Tony's Finer Foods, Chicago, IL. Dissected otoliths were cleaned with fine forceps, bleached briefly with 0.65% wt/vol sodium hypochlorite (Secor et al. 1991), sonicated in deionized water (conductivity > 18 MΩ/cm), and rinsed with a dental water jet. Trout otoliths for mass spectrometry were not bleached.

Isolation and electrophoresis of otolith proteins

Otoliths were dissolved with a two-fold excess of EDTA in the presence of protease inhibitors (cOmplete; Roche Diagnostics, Indianapolis, IN), and insolubles were pelleted by centrifugation at 16,100 × g for 15 min at 4°C. The buffer of the soluble fraction was exchanged for a denaturing solution containing 7 M urea, 2% wt/vol 3-[(3-Cholamidopropyl)dimethylammonio]-1-propanesulfonate hydrate (CHAPS), 0.5% wt/vol Zoom carrier ampholytes 3-10 (Invitrogen,

Carlsbad, CA), protease inhibitors, 8 mM Tris, and 7.5 mM HCl (final pH 7.0-7.2) by ultracentrifugation with a nominal cut-off of 10 kDa; the insoluble pellet was taken up in the same solution. After alkylation with iodoacetamide, 4x NuPAGE LDS sample buffer (Invitrogen) and dithiothreitol were added to final concentrations of 1x and 48 mM, respectively, and the samples were electrophoresed through precast NuPAGE Bis-Tris 4-12% polyacrylamide gels in a 2-(N-Morpholino) ethanesulfonic acid (MES) running buffer containing sodium dodecylsulfate and NuPAGE antioxidant (Invitrogen). The separated proteins were visualized with a SilverQuest staining kit (Invitrogen).

Mass spectrometry

Otoliths were dissolved as above, with the addition of 2.5 mM Tris(2-carboxyethyl) phosphine hydrochloride. Soluble protein was precipitated (UPPA concentration kit; Genotech, St. Louis, MO) and quantitated in a membrane-based fluorescence assay (EZQ kit; Molecular Probes, Eugene, OR). After alkylation with iodoacetamide, the protein was digested with proteomics-grade trypsin (Genotech) at 55°C for 15 min in a microwave incubator (Discover Digestor; CEM, Matthews, NC).

The tryptic peptides were separated by reverse-phase high-pressure liquid chromatography on an Atlantis dC18 NanoEase column (3 μm particle size, 75 μm x 150 mm; Waters, Milford, MA) with a 60-min gradient of 0%-50% vol/vol acetonitrile containing 0.1% vol/vol formic acid at a flow rate of 250 nl/min and analyzed on-line with a Waters Q-ToF API-US tandem mass spectrometer (Protein Sciences Facility, Biotechnology Ctr., Univ. of Illinois).

A custom database of chordate proteins was compiled from all sequences that were available from the National Center for Biotechnology Information as of 12/5/2006, including

GenBank (release 156), or that were associated with fish genomes in Ensembl (release 41): medaka (assembly HdrR), green puffer (assembly TETRAODON 7), stickleback (assembly BROAD S1), fugu (assembly FUGU 4.0), and zebrafish (assembly Zv6). Redundancies were removed with the WU-BLAST patdb utility, and the reversed sequences added as decoys. The final database contained 844,832,953 residues in 2,106,626 entries.

Peak lists were generated from the monoisotopic mass spectra filtered with ProteinLynx Global Server vs. 2.2.5 (Waters) and analyzed with two complementary procedures: Mascot vs. 2.2.03 (Pappin et al. 1993; Matrix Science, Boston, MA) was used for error-tolerant ion searches with a peptide mass tolerance of ± 2 Da, a fragment mass tolerance of ± 0.8 Da, carbamidomethyl-cysteine as fixed modification, and no more than two missed trypsin cleavages; this procedure matches spectra in a single step directly to database sequences, but relies on the underlying protein or a close homolog being represented in the database. Alternatively, PEAKS (Ma et al. 2003; Bioinformatics Solutions, Waterloo, ON) was used to interpret the peak lists *de novo,* with peptide and fragment mass tolerances of ± 0.1 Da. The predicted peptide sequences were then used as queries in MS-BLAST searches (Shevchenko et al. 2001) with WU-BLAST 2.0 [16-Jun-2004] (Korf et al. 2003; Lopez et al. 2003). This procedure is less integrated than Mascot, but may be more sensitive for species such as trout and catfish with fewer known proteins.

To assess the statistical significance of each database match, we calculated an Expect value, the number of times a match of the same quality was expected to occur by chance in a database of the same size. For Mascot, Expect values were based on the highest peptide Mowse score; for PEAKS/MS-BLAST, Expect values were based on a survival curve (Fenyö and Beavis 2003) of the BLAST *E*-values of the decoy matches. Database matches from the automated

Mascot and PEAKS/MS-BLAST procedures with at least two matching peptides and Expect values below 0.05 were analyzed further. Groups of orthologous proteins were reduced to a single match with the lowest Expect value. Peptides that lacked flanking K or R residues, had mass errors larger than 0.1 Da, missed more than one internal cleavage, or failed to identify the same protein on their own in a BLASTP search against the current non-redundant GenBank database were eliminated, and the search statistics were recalculated.

RT-PCR

First-strand cDNA synthesis from total zebrafish RNA was primed with oligo$(dT)_{18}$. Amplifications were cycled 30 times with an annealing temperature of 55°C and contained cDNA corresponding to 5 to 12.5 ng total RNA per μl and 0.2 μM of each primer (5' to 3'): *sparc* exons 4 and 6, TTGAGGTCGTGGAGGATGTT & GTATTTGCAGGGTCCGATGT; *bactin1* exons 1 and 2, TCTTCACTCCCCTTGTTCAC & GCATCATCTCCAGCAAAACC.

In situ hybridization

The coding region of zebrafish *sparc* in pBluescript II SK(+) (Stratagene, La Jolla, CA) was amplified with flanking M13 primers and used as a template to synthesize digoxigenin-labeled riboprobes with T3 (antisense) or T7 (sense) RNA polymerase. Hybridizations were conducted as described (Thisse and Thisse 2008). No labeling was detected in control experiments with sense probe.

Antibody production

The coding sequence for mature zebrafish Sparc was amplified with the primers GACTCCATGGGCGCTCCAACTGAAGAGGAGCCAGCT and

GACTCGGCCGCGATGACAAGGTCTTTGTCGACATC and inserted at the *Nco*I and *Eag*I sites of the vector pET-28a(+) (Novagen, Madison, WI). The resulting fusion protein with a C-terminal His_6-tag was purified as described (Kollmar et al. 2001) and used to generate polyclonal antiserum UI-37 in rabbits.

Protein immunoblotting

A crude bone extract from trout was prepared as described (Fisher et al. 1987). Purified bovine SPARC (osteonectin) was purchased from Haematologic Technologies, Essex Junction, VT. Total protein from whole zebrafish embryos was isolated with TRIzol reagent (Invitrogen). Proteins were electrophoresed as above, and blotting and detection were as described (Kollmar et al. 1997), except that blocking buffer was StartingBlock (Pierce Biotechnology, Rockford, IL) and detection was based on fluorescence. The primary antibodies were BON-1, a rabbit polyclonal antiserum against purified bovine SPARC at a dilution of 1:5,000 (Ingram et al. 1993); E7, ascites fluid containing a mouse monoclonal antibody against β-tubulin at 0.2 μg/ml IgG (Chu and Klymkowsky 1989; Developmental Studies Hybridoma Bank, Iowa City, IA); and UI-37 (see above) at 1:1,500. The secondary antibodies were donkey anti-rabbit and anti-mouse IgG antibodies conjugated to IRDye 680 or 800CW (LiCor, Lincoln, NE), respectively, at 67 ng/ml in the presence of 0.01% (wt/vol) sodium dodecylsulfate. Membranes were scanned with a two-channel Odyssey Infrared Imaging System (LiCor); fluorescence intensity varied linearly with the amount of protein from 24 to at least 3,000 fluorescence units (r^2 = 97%).

Immunofluorescence

Zebrafish embryos were labeled as described (Jowett 1999, protocol 6.12; Starr et al. 2004). Lapilli from adult zebrafish were cut with a scalpel into slices of 120-300 μm thickness, etched

for two hours with 17 mM acetic acid, post-fixed for 30 min, and labeled without permeabilization. Primary reagents were UI-37 or preimmune serum diluted 1:200 or normal rabbit IgG at 11 μg/ml (Jackson ImmunoResearch Laboratories, West Grove, PA); secondary reagents were 2.5 μg/ml 4',6-diamidino-2-phenylindole (DAPI) and 2.5 μg/ml Alexa-Fluor-488-conjugated donkey anti-rabbit IgG or 165 nM Alexa-Fluor-488-conjugated phalloidin (Molecular Probes). Stacks of fluorescence images were acquired under structured illumination (Apotome; Carl Zeiss, Thornwood, NY), and maximum-intensity projections in the z-axis prepared with ImageJ (Wayne Rasband, National Institutes of Health, Bethesda, MD).

Morpholino injections

The morpholinos (5' to 3', mismatches in lower case) ATG-MO, ATCTTGAGTTTCAGCCTTCTGTCCG (Eckfeldt et al. 2005); ATGmis-MO, ATgTTcAGTTTgAGCCTTgTGTgCG; e5i5-MO, GGAATGAGAAAAGACACGCACATGC; e5i5mis-MO, GGAATcAGAAAAcACACcCAgATcC; and Std-MO CCTCTTACCTCAGTTACAATTTATA (Gene Tools, Philomath, OR) were injected as described (Gilmour et al. 2002). Working dilutions were prepared in vehicle comprising Danieau buffer, 0.05% (wt/vol) phenol red, and 2.5 mg/ml tetramethylrhodamine dextran 10,000 MW (Molecular Probes); 1 nl per embryo was injected at the one-cell stage. The order of treatments was randomized for each experiment. Dead and non-fluorescent embryos were removed after one day; the fraction of fluorescent embryos among survivors ranged from 33% to 100% with a median of 86%. At 28, 52, and 76 ± 0.5 hours post fertilization (hpf), a random sample of 12 to 16 embryos was removed from each treatment group for microscopy and subsequent fixation or RNA and protein isolation.

Morphant analysis

For otolith measurements, anesthesized embryos were mounted in 3% (wt/vol) methylcellulose in E2 medium (Kane and Kishimoto 2002), and the otic vesicles were imaged on a compound microscope. The otolith and otic-vesicle areas were outlined manually with Axiovision 4.6 (Carl Zeiss). For scanning electron microscopy, otoliths were dissected from embryos fixed with 85% vol/vol ethanol, mounted dry on conductive carbon adhesive tape, and sputter-coated with gold/palladium. For semi-thin sections, embryos fixed in BT fix (Westerfield 2000) were embedded in LR White resin hard grade (Electron Microscopy Sciences, Hatfield, PA), sectioned at 1 μm thickness with a diamond knife on an ultramicrotome, and stained with toluidine blue (Richardson et al. 1960). Startle responses were examined as described (Kappler et al. 2004). Analysis of variance and *post-hoc* Bonferroni comparisons were conducted with Minitab 15 (Minitab, State College, PA).

Results

Three novel otolith proteins identified by mass spectrometry

To identify unknown otolith proteins in an efficient and comprehensive fashion, we analyzed crude extracts of trout and catfish otoliths by tandem mass spectrometry in a shotgun approach. We chose these species because they are farmed commercially and easily available, their otoliths weigh tens to hundreds of milligrams *versus* the tens of micrograms in laboratory species such as the zebrafish, and their complements of otolith proteins appear to be similar to those of a wide range of actinopterygii (Fig. 1). We chose crude extracts to avoid the losses associated with separating minute amounts of proteins and because the otolith "proteome" comprises only about two dozen proteins (Fig. 1). From 10 mg of adult trout or catfish otoliths as starting material, we extracted about 2 μg each of EDTA-soluble protein under reducing conditions. After digestion with trypsin and separation of the resulting peptides by liquid chromatography, we obtained 571 mass spectra from trout and 392 from catfish; the smaller number may have been due to the use of hypochlorite for otolith cleaning and resulted in fewer database matches.

To analyze the spectra, we employed two complementary procedures, Mascot and PEAKS/MS-BLAST, to search a comprehensive database of chordate proteins. If the top database match for a group of orthologous proteins was from a different species than the otolith extract, it was used as a query for *post-hoc* BLAST searches to find matching trout or catfish nucleotide sequences. We thus identified three novel otolith proteins with statistically significant database matches (Table 1).

The first novel otolith protein was Sparc, a Ca^{2+}- and collagen-binding protein and major constituent of bone and dentin. Its closest paralog, SPARC-like 1, has been found in mouse otoconia (Thalmann et al. 2006). However, the peptide sequences predicted by PEAKS from

trout otolith spectra were far more similar to trout Sparc than to trout Sparcl, the ortholog of mouse SPARC-like 1 (Table 2). Similarly, the PEAKS predictions from catfish were more similar to zebrafish Sparc than to zebrafish Sparcl (data not shown).

The second was precerebellin-like protein (Cblnl), a member of the family of C1q-domain-containing proteins that includes collagen types VIII and X and otolin-1. Of the five tryptic Cblnl peptides matched by Mascot and PEAKS/MS-BLAST, two were more similar to isoform a and two were more similar to isoform b (Table 3), suggesting that two Cblnl isoforms are present in otoliths. The underlying nucleotide sequences were about 90% identical; we could not determine whether the isoforms arose from alternative splicing, polymorphisms, or separate genes.

The third was neuroserpin (Serpin I1), a member of the large family of serine-protease inhibitors. Mascot and PEAKS/MS-BLAST identified the zebrafish and the medaka ortholog, respectively, as the top match. A *post-hoc* BLAST search identified a set of expressed sequence tags (ESTs) that encoded trout neuroserpin; their conceptual translation matched the PEAKS predictions from trout otolith spectra better than any other serpin (data not shown).

In addition, we also observed three of the four known otolith proteins—otolith matrix protein-1, otolin-1, and otolith matrix macromolecule-64—with one to twelve matching peptides, 5% to 59% coverage, and Expect values between 0.082 and $1.5 \cdot 10^{-13}$ (data not shown). The three novel and three known otolith proteins were the only database matches with significant Expect values, other than the common contaminants human keratin and porcine trypsin. The concordance and statistics of the Mascot and PEAKS/MS-BLAST results strongly support the identification of Sparc, precerebellin-like protein, and neuroserpin as otolith proteins.

Sparc is a constituent protein of zebrafish otoliths

Sparc was found in both trout and catfish otoliths in our proteomics study (Table 1) and has a well-established role in bone formation (Brekken and Sage 2000). We, therefore, set out to test the hypothesis that Sparc also plays a role in otolith morphogenesis. We started by investigating its expression in the zebrafish, an animal model that is more tractable for embryological and genetic studies than trout or catfish.

The level of *sparc* mRNA was seen to step up around 9 hpf, near the end of gastrulation, in a qualitative RT-PCR assay with whole zebrafish embryos (Fig. 2A). At 14 hpf, *sparc* mRNA was located in the otic placode of zebrafish embryos by *in situ* hybridization; the signal was stronger than anywhere else, including somites and floorplate (see Fig. 2B and data not shown; for the anatomy of the developing zebrafish ear, see Haddon and Lewis 1996; Whitfield et al. 2002). Within the otic vesicle at 28 hpf, the mRNA became more regionalized (Fig. 2C); at 52 hpf, it was concentrated in one domain marking the sensory maculae and in another marking the developing semicicular canals (Fig. 2D). At least until 7 dpf, the mRNA level in the ear remained comparable to that in other areas of the body, such as the notochord (data not shown; see also Thisse B, Thisse C. Fast release clones: a high throughput expression analysis. ZFIN Direct Data Submission, http://zfin.org, 2004; Rotllant et al. 2008). The expression of the *sparc* gene in the ear thus commences long before the seeding period of otolith formation begins around 18 hpf.

To verify the presence of Sparc in otoliths, we first conducted protein immunoblotting experiments. In a crude extract of zebrafish otoliths, a single protein was detected by antiserum UI-37 raised against recombinant zebrafish Sparc in our laboratory (Fig. 2E). The protein's mobility corresponded to the apparent molecular mass of 39 kDa typical for reduced Sparc (Sage

2003) and matched that of a band of intermediate intensity in a silver-stained gel slice (Fig. 2E). Control experiments demonstrated that the UI-37 serum bound to Sparc in a specific manner: Binding was impervious to preadsorption of the serum with a plain bacterial extract, but was blocked by preadsorption with a bacterial extract containing recombinant zebrafish Sparc; no signal was observed with preimmune serum, with purified naive rabbit IgG, or without primary antibody (Fig. 2E). Furthermore, both UI-37 and BON-1, an antiserum against bovine SPARC, detected a single protein of the same mobility in extracts from trout otoliths and bone and bound to purified bovine SPARC (data not shown).

Next, we located Sparc in the ears of zebrafish embryos by whole-mount immunofluorescence labeling. At 28 hpf, antiserum UI-37 detected Sparc at the surface of both otoliths and throughout the epithelium that lines the otic vesicle (Fig. 2F); the latter signal was strongest at the caudal end, matching the distribution of the *sparc* mRNA (Fig. 2C). The specificity of Sparc recognition by UI-37 was demonstrated by using the same controls as for immunoblotting above (Fig. 2G and data not shown). This result demonstrated that Sparc is incorporated into otoliths already at the earliest stage of their life-long growth phase.

Finally, to demonstrate that the Sparc detected above was not an accidental contaminant from adhering tissue or extracellular matrix, we examined cross-sections of adult zebrafish otoliths by immunofluorescence microscopy. Fluorescent labeling was observed with UI-37 serum (Fig. 2H-I). The same control experiments as for immunoblotting above demonstrated the specificity of the labeling (Fig. 2J-K, L-M, and data not shown). Together, these expression studies confirmed and extended our proteomics results and demonstrated that Sparc is a true constituent of otoliths.

Diminished Sparc expression in zebrafish morphants

To manipulate the level of Sparc expression, we turned to injecting antisense morpholino oligonucleotides ("morpholinos") into zebrafish embryos ("morphants"). The first morpholino was designed to block translation by binding to the 5'-UTR and start codon of the *sparc* mRNA (Fig. 3A, ATG-MO). The second morpholino was designed to block splicing by binding to the donor site at the junction of exon 5 and intron 5 (Fig. 3A, e5i5-MO). Morpholinos with five nucleotide mismatches (ATGmis-MO, e5i5mis-MO) or directed against a mutant human β-globin mRNA (Std-MO) were used as negative controls. To find optimal concentrations, we titrated the morpholinos over a range of 0.46-4.5 ng per embryo. ATG-MO and e5ie-MO doses above 1 ng induced the otolith abnormalities described below in a reproducible and dose-dependent manner (data not shown). Above 4 ng, however, most embryos died by three days of age. We, therefore, chose 2.0 and 2.4 ng per embryo as the optimal doses for ATG-MO and e5i5-MO, respectively.

To verify that the morpholinos targeted Sparc, we measured their effect on mRNA and protein levels. After injection of 2.4 ng e5i5-MO per embryo, RT-PCR with flanking primers in exons 4 and 6 detected multiple splice isoforms at 28, 52, and 76 hpf in two independent experiments (Fig. 3B and data not shown). We were able to sequence four isoforms: The first originated from a cryptic splice donor site inside exon 5 *(*a in Figs. 3A-B), the second from the normal donor site at the exon-intron junction (b), the third from a cryptic donor site inside intron 5 (c), and the fourth retained all of intron 5 (unspliced). The deletion in isoform a and the insertion in c were in-frame, encoding peptides with 26 additional or 12 missing amino acids, respectively. The most abundant, unspliced isoform encoded a foreshortened 112-amino-acid

peptide because of a premature stop codon in intron 5. In contrast, only the wild-type isoform b was detected after injecting negative controls (Fig. 3B).

A major reduction of Sparc protein after injecting 2.0 ng ATG-MO or 2.4 ng e5i5-MO per embryo was revealed by two-color immunofluorescence blotting with the UI-37 antiserum and a mouse monoclonal antibody against β-tubulin (Figs. 3C-D). Based on quantitation within the linear range of the fluorescence signal, the Sparc content in ATG- and e5i5-morphants at 28 to 76 hpf was reduced between 7- and 44-fold when compared to controls of the same age (Fig. 3D). In contrast, the β-tubulin content varied at most by a factor of 2.4 among samples of the same age (Fig. 3C and data not shown). In ATGmis-MO and e5i5mis-MO controls, the Sparc content was also reduced when compared to vehicle- and Std-MO controls, but no more than two-fold; these small effects may have been due to the finite affinities of the mismatch morpholinos. The abnormal Sparc peptides predicted from the misspliced mRNAs in the e5i5-morphant were not observed, suggesting that they were unstable. Together, the RT-PCR and immunoblotting results indicated a substantial and specific reduction of Sparc levels in ATG- and e5i5-morphants.

Sparc is required for normal otolith growth

To assess the functional requirement for Sparc in otolith formation, we analyzed otolith morphology at 28, 52, and 76 hpf for ATG- and e5i5-morphants in three independent experiments each. In wild-type otic vesicles observed live under brightfield illumination, a pair of spheroidal otoliths is visible at each age in stereotypic locations, the anterior lapillus and the posterior sagitta (Fig. 4A). In both ATG- and e5i5-morphants, we consistently observed abnormalities regarding four attributes (Fig. 4B-D): size (smaller otoliths), shape (fused otoliths), location (ectopic otoliths), and number (missing or up to three extra otoliths). Fused otoliths were

sometimes difficult to distinguish and therefore not tallied separately. However, dissection and scanning electron microscopy confirmed that fused and smaller otoliths were not artifacts of the fixed perspective under the light microscope (Fig. 4E-I). Ectopic otoliths were usually located close to the anterior or posterior macula and appeared to be attached. Sectioning revealed a striking difference between wild-type and morphant otoliths: In the former, a small, dark core was surrounded first by thick, light layers of striated, mineralized matrix and then by a thin, dark, unmineralized rim with a distinct margin (Fig. 4J). In the latter, the core, mineralized matrix, and rim were much smaller and occasionally enclosed by an additional, proteinaceous layer. Furthermore, the entire assembly stained more darkly, suggesting a higher ratio of protein to $CaCO_3$ in morphant otoliths (Fig. 4K).

Smaller size was by far the predominant phenotype and occurred often alone. To quantify its prevalence, the total otolith area visible under brightfield illumination was measured (Fig. 4L). The mean of the total otolith area in both morphants, as determined by analysis of variance, was about half that of vehicle- or Std-MO-injected controls. These differences were highly significant and mirrored the diminished Sparc expression reported above (Fig. 3D). In ATGmis- and e5i5mis-morphants, the mean was also reduced, but the effect was far less pronounced. Furthermore, individual otoliths in morphants were never abnormally large. In particular, ectopic otoliths were usually smaller than the lapillus and sagitta in the same otic vesicle, and even fused otoliths were rarely larger than the mean in controls of the same age. These results suggested a requirement for Sparc in otolith growth.

The other abnormalities frequently occurred in combination, such as an extra, ectopic otolith (Fig. 4C) or a missing otolith fused to another (Fig. 4D). To quantify their prevalence, embryos were classified according to the presence or absence of lapillus and sagitta; each group

was then subdivided according to the absence or presence of ectopic otoliths (Table 4). The proportion of each phenotype was similar in the two morphant types. Almost all morphants retained both a lapillus and a sagitta in its normal location. Extra otoliths were more common than partially or completely missing otoliths. The probabilities of loosing either the lapillus or the sagitta were almost equal (4% *vs*. 3% when averaged over all ages). The percentage of abnormal otolith numbers decreased with age, regardless of treatment.

Sparc plays a direct role in otolith growth

Consistent with the widespread expression of Sparc, we observed abnormalities elsewhere in the ATG- and e5i5-morphants, such as defective otic vesicles and twisted fins. The survival after one week of the morphants, but not of the mismatch- or Std-MO-injected controls, was significantly lower than that of the vehicle-injected controls (37%±6% *vs*. 67%±5%, mean ± SEM, $P = 0.01$ with 17 df). Similarly, the fractions of spontaneously (31%±6%) or upright (62%±5%) swimming morphant larvae at one week of age were significantly lower than those of the vehicle-injected controls (70%±9% and 95%±3%, $P = 0.02$ and 0.001, respectively, with 17 df), whereas the fractions exhibiting a startle response to sound were indistinguishable (96%±2% *vs*. 100%±3%); these differences may have been due to the fin defects or to vestibular dysfunction.

The otic-vesicle abnormalities in morphants included smaller size and disrupted semicircular canals, but did not extend to features associated with otoliths, such as the morphology of the anterior macula (Fig. 4J-K) or its number of hair bundles (Fig. 4M-N). Furthermore, whereas the otolith defects were equally severe in the ATG- and e5i5-morphants (see above), the otic-vesicle defects were much milder in the latter. While the epithelial projections forming the semicircular canals at later stages (52 and 76 hpf) were less prominent in e5i5-morphants than in vehicle- or Std-MO-injected controls, the overall appearance of the otic

vesicle was often indistinguishable (see Fig. 4A *vs*. B-D); the exception were otic vesicles without any otoliths, which were always tiny and looked grossly abnormal. This impression was confirmed quantitatively by analysis of variance of the visible otic-vesicle area as a proxy for size: ATG-morphants, but not e5i5-morphants, had significantly smaller vesicles than control embryos (Table 5). These observations were consistent with the higher residual Sparc levels in e5i5- than in ATG-morphants (Fig. 3D).

To assess whether Sparc knockdown affected otolith growth directly or indirectly, via defects in otic-vesicle development, we focussed on the predominant phenotype, smaller otoliths, in isolation. Plotting otolith size against otic-vesicle size for embryos with only a properly-located lapillus and sagitta revealed a weak linear correlation in vehicle- and Std-MO-injected embryos at 52 and 76 hpf (Fig. 4O and data not shown). ATG- and e5i5-morphants also displayed linear correlations, but with much smaller intercepts. At any given otic-vesicle size, the mean otolith size was thus always substantially smaller in morphants than in controls. Together, these observations demonstrated that otolith growth in Sparc morphants is reduced regardless of the severity of otic-vesicle defects and suggested that Sparc plays a direct role in otolith growth.

Discussion

Our mass-spectrometry analysis revealed the presence of Sparc, precerebellin-like protein, and neuroserpin in trout and catfish otoliths. None of these proteins had been associated previously with otolith or otoconia formation. Immunodetection confirmed independently that Sparc is a true constituent of trout and zebrafish otoliths. Finally, knockdown of Sparc expression in morphant zebrafish resulted in four principal types of defective otoliths: smaller, extra and ectopic, missing and fused, or completely absent. Smaller size was the predominant phenotype and independent of the severity of otic-vesicle defects. These results suggested that Sparc is directly required for normal otolith growth.

By taking a shotgun proteomics approach, we almost doubled the number of known otolith proteins. Previously, constituent otolith proteins had been isolated one at a time by electrophoresis (Murayama et al. 2000; Murayama et al. 2002), database searches (Söllner et al. 2003; Petko et al. 2008), or immunoscreening (Tohse et al. 2008). Recently, Zhao and colleagues (2007) employed mass spectrometry to detect three proteins in a crude extract from mouse otoconia: otoconin 90 (Wang et al. 1998; Verpy et al. 1999) and fetuin-A (Thalmann et al. 2006) as well as otolin-1, whose ortholog had previously been isolated from salmon otoliths (Murayama et al. 2000). We identified three new and three out of four known otolith proteins concurrently by taking advantage of a rich source—the large otoliths of commercially farmed species—and the recent advances in proteomics technology (Domon and Aebersold 2006). This strategy may be useful in general for studying tissues or organs that are too small in laboratory species, such as the zebrafish, to yield sufficient material. Even with seven known constituents, though, the catalog of otolith proteins is unlikely to be complete yet. Further advances may

require additional sample treatments, such as deglycosylation or harsher fragmentation, especially for the insoluble fraction, before mass spectrometry.

Sparc, the first otolith protein we identified, is a multifaceted molecule with a broad range of physiological effects. It occurs in most basement membranes, dentin, cartilage, and bone of vertebrates, where it constitutes up to 23% of total protein by weight (Termine et al. 1981; Brekken and Sage 2000). It belongs to the matricellular proteins that modulate the assembly and maintenance of the extracellular matrix, but do not provide structural support (Bradshaw and Sage 2001). Rotllant and colleagues (2008) have recently shown that Sparc is required for the morphogenesis of pharyngeal cartilage and for later stages of inner-ear development in zebrafish, but do not report on otolith abnormalities in their morphants. Sparc knockout mice exhibit, among other defects, curly tails and a weaker skin (Bradshaw et al. 2003), a reduced foreign-body reaction (Puolakkainen et al. 2003), accelerated vertebral disc degeneration (Gruber et al. 2005), and reduced bone mass and strength (osteopenia) despite normal development of the skeleton overall (Gilmour et al. 1998; Delany et al. 2000; Boskey et al. 2003); in each case, the associated molecular abnormalities include an altered collagen ultrastructure. Sparc acts on the extracellular matrix both directly and indirectly: A C-terminal extracellular Ca^{2+}-binding module also binds to collagen and may provide a chaperone or escort function during secretion and assembly, and an internal follistatin-like module influences the proliferation, differentiation, and adhesion of surrounding cells (Bradshaw and Sage 2001; Martinek et al. 2007; Rentz et al. 2007). Because of the affinity of its N-terminal acidic module for both Ca^{2+} and hydroxyapatite, Sparc may also act as a linker between collagen and the mineral phase in bone and promote mineralization. *In vitro,* however, Sparc has been variously

found to stimulate (Termine et al. 1981), inhibit (Romberg et al. 1986; Doi et al. 1989), or not at all affect (Hunter et al. 1996) hydroxyapatite formation, leaving this hypothesis unresolved.

Sparc belongs to a group of homologous proteins with important roles in tissue mineralization. Its closest paralog Sparc-like (Sparcl) gave rise, via gene duplications, to the secreted calcium-binding phosphoproteins (Kawasaki and Weiss 2006) that include the otolith or otoconia proteins starmaker (Söllner et al. 2003), otolith matrix macromolecule-64 (Tohse et al. 2008), and osteopontin (Sakagami 2000; Thalmann et al. 2006; Zhao et al. 2008). Sparc-like itself, which is about twice the size of and 50-70% identical to Sparc, has been found in mouse otoconia (Thalmann et al. 2006. We cannot exclude the possibility that Sparc-like is also present in otoliths; however, we did not detect *sparcl* mRNA in the developing zebrafish ear by *in situ* hybridization (Y.-J.K., A.S., & R.K., unpublished). In contrast, we and others have observed a strong and specific signal for *sparc* mRNA in the ear of zebrafish and medaka embryos (Thisse and Thisse 2004; Renn et al. 2006; Nemoto et al. 2008; Rotllant et al. 2008). Furthermore, the sequence alignments of our mass-spectra predictions and our immunodetection experiments clearly identified Sparc as a constituent of otoliths. The secreted calcium-binding phosphoproteins appear to have diverged and exchanged roles throughout the vertebrate lineage (Kawasaki and Weiss 2006). In a similar fashion, Sparc and Sparc-like may perform the same role in otoliths and otoconia, respectively.

The otolith abnormalities in our Sparc morphants encompassed all the main phenotypes of otoconin 90 (smaller, extra, or missing; Petko et al. 2008), otolith matrix protein (smaller; Murayama et al. 2005), and otolin-1 (fused; Murayama et al. 2005), but appeared to be opposite to that of starmaker (reduced vs. enhanced mineralization; Söllner et al. 2003). This would be

consistent with, but not proof of genetic or physical interactions between Sparc and some or all of these otolith proteins.

Sparc's multifaceted nature and widespread expression raise the question whether the otolith abnormalities in the morphants were a non-specific consequence of earlier defects elsewhere in the body. Based on the expression patterns of molecular markers, knockdown of Sparc expression in zebrafish morphants does not perturb early ear development, until 24 hpf, and later defects are not due to general retardation (Rotllant et al. 2008). This conclusion should extend to otolith growth, which occurs late in ear development. Furthermore, our morpholino doses were lower than those of Rotllant and colleagues (0.2-0.3 *vs*. 0.5-1 pmol per embryo), and the survival rate of our morphants at 7 dpf was higher (36% *vs*. <20%); non-specific effects in our morphants should thus be even less pronounced than in their study.

Consideration of the critical seeding period of otolith formation between 18.5 hpf and 24 hpf (Riley et al. 1997) further supports a later time frame for the effects of Sparc knockdown. During this seeding period, diffusible seeding particles must attach to tether cells in the anterior and posterior macula to initiate the subsequent life-long growth period of a properly-located lapillus and sagitta, respectively. Tethering defects characteristically lead to the formation of a single, oversized otolith, with a preferential loss of the lapillus over the sagitta (Riley et al. 1997; Riley and Moorman 2000; Sumanas et al. 2003). In contrast, we observed both a lapillus and a sagitta in their proper locations in 80%-96% of our Sparc morphants. In the small fraction of animals with a single otolith, lapillus and sagitta were lost with almost equal probability. Lack of seeding or tethering is, therefore, unlikely to underlie the majority of abnormal otoliths in Sparc morphants.

To distinguish between direct and indirect effects of Sparc knockdown, we focused on the smaller-size phenotype, which predominated and often occurred alone, and the period of otolith growth after 24 hpf. Two lines of evidence argue against an indirect consequence of otic-vesicle defects. First, our demonstration that Sparc protein is a true constituent of otoliths suggested a direct role in their morphogenesis. It seems unlikely that the incorporation of Sparc at all ages from embryo to adult is purely adventitious. Second, the comparison of our ATG- and e5i5-morphants suggested that otolith size and otic-vesicle phenotype were independent. Rotllant and colleagues (2008) reported three characteristic and specific anatomical defects of otic-vesicles in Sparc morphants at 68 hpf: a markedly smaller ear, closer apposition of the anterior and posterior macula, and disrupted formation of the semicircular canals. In our observations at 52 and 76 hpf, we detected a much milder otic-vesicle phenotype in the e5i5-morphants—no significant difference in otic-vesicle size from control embryos and no displacement of the maculae, as judged from the locations of lapillus and sagitta. Only the semicircular canals were abnormal, which form a separate domain of Sparc expression from the maculae and are not thought to be involved in otolith formation. Otolith size, in contrast, was reduced just as significantly in the e5i5-morphants as in the ATG-morphants with a more severe otic-vesicle phenotype. While it is fundamentally impossible to rule out all other explanations, our results indicate a requirement for Sparc in otolith growth that is specific, direct, and independent from its role in otic-vesicle development. At the molecular level, morphant otoliths may be smaller and their mineral phase reduced because the collagenous otolin-1 or other structural proteins are not properly assembled into a framework in the absence of Sparc; alternatively, the $CaCO_3$ may not be properly deposited on or linked to the framework without Sparc.

Because the other otolith abnormalities in Sparc morphants occurred less frequent and in numerous combinations, we can interpret them only tentatively. Extra, ectopic otoliths, the second-most common phenotype, may have resulted from a reduction in the stickiness that allows seeding particles to fuse with a tethered lapillus or sagitta (Riley et al. 1997) and that may also underlie the decreasing frequency of extra otoliths with age in both morphants and controls. This stickiness could depend on Sparc's direct participation in framework assembly or mineralization at the otolith surface. The rare opposite phenotype of missing single otoliths, in contrast, likely arose from Sparc's role in otic-vesicle development. Its frequent coincidence with fused otoliths suggests a closer apposition of the anterior and posterior macula or impaired tethering as the underlying cause. Finally, the tiny and grossly abnormal otic vesicles accompanying the occasional lack of any otoliths make it impossible to distinguish between non-specific, indirect, and direct effects for this phenotype. We conclude that only a small fraction of the abnormal otoliths in morphants should be attributed to indirect rather than direct effects of Sparc knockdown.

Precerebellin-like (Cblnl), the second new otolith protein we identified, may partner with Otolin-1 during framework assembly. Trout Cblnl contains a secretory signal peptide and a globular C1q domain; its structure thus resembles those of collagens VIII and X and of Otolin-1, except that it lacks their collagen-like region (Gerwick et al. 2000; Tom Tang et al. 2005; Mei and Gui 2008). The short-chain collagens VIII and X assemble into a reticular network with hubs formed by trimers of C1q domains and spokes formed by collagen fibrils (Kwan et al. 1991; Sutmuller et al. 1997). The insoluble protein fraction of otoliths also forms a reticular network (Zhang 1992). Cblnl could thus be associating with Otolin-1 via their C1q domains and reduce the connectivity of the internal hubs or cap the hubs at surfaces.

Neuroserpin (SerpinI1), the third new otolith protein we identified, may also be involved in framework assembly. It is a secreted member of the large family of serine-protease inhibitors and a modulator of proteolytic cascades (Miranda and Lomas 2006). One of its key substrates is tissue plasminogen activator, a serine protease that converts other proteases into their active form, such as the eponymous plasminogen into plasmin. In bone, plasmin activates matrix metalloproteases with collagenase activity during various stages of development or resorption (Varghese 2006). For example, the conversion of cartilage to bone (endochondral ossification) involves the proteolysis of collagen X, a close paralog of otolin-1, and its replacement by calcium phosphate (Ballock and O'Keefe 2003; Shen 2005). Intriguingly, Sparc anchors tissue plasminogen activator to collagen and enhances local plasmin activity (Kelm et al. 1994). Neuroserpin and Sparc could thus be localizing and regulating protease activity together during otolith formation.

In summary, we have identified three new otolith proteins that may interact with the collagenous otolin-1 during framework assembly and mineralization. Future studies to test this hypothesis will need to examine the location and function of precerebellin-like protein and neuroserpin as we did for Sparc, the ultrastructure of the extracellular matrix, and the dynamic associations among these three proteins and Otolin-1 in wild-type and morphant zebrafish. Because of their acellular structure, otoliths could complement the more complicated bone and tooth as a model system for dissecting Sparc's roles in biomineralization.

Acknowledgments

We thank Ms. Janie Harder (Idaho Trout Co.), Dr. Mark Nelson (Dpt. of Mol. and Int. Physiol., Univ. of Illinois), Dr. Geoffrey Waldbieser (USDA/ARS), and Mr. Doug Wojcieszak (Illinois Fish Farmers Coop.) for fish heads; Dr. Larry Fisher (NIH/NIDCR) for antiserum BON-1; Ms. Liping Wang and Ms. Rachel Breitenfeld (Immunol. Resource Ctr., Univ. of Illinois) for antibody production; Ms. Domenika Kurek, Mr. Scott Malm, and Mr. Timothy Smith for help with morpholino injections and otolith measurements; Mr. Scott Robinson and Ms. Cate Wallace (Imaging Technol. Group, Beckman Inst., Univ. of Illinois) for advice on ultramicrotomy and help with scanning electron microscopy; and Mr. Kurin Iimura, Dr. Rena Orman, and Dr. Mark Stewart for comments on the manuscript. R.K. dedicates this manuscript to Prof. Dr. A. J. Hudspeth in gratitude for his erstwhile support. This work was supported by startup funds from the University of Illinois and National Institutes of Health grant DC006962 to R.K.

References

Ballock RT, O'Keefe RJ. The biology of the growth plate. J Bone Joint Surg Am 85-A: 715-726, 2003.

Boskey AL, Moore DJ, Amling M, Canalis E, Delany AM. Infrared analysis of the mineral and matrix in bones of osteonectin-null mice and their wildtype controls. J Bone Miner Res 18: 1005-1011, 2003.

Bradshaw AD, Sage EH. SPARC, a matricellular protein that functions in cellular differentiation and tissue response to injury. J Clin Invest 107: 1049-1054, 2001.

Bradshaw AD, Puolakkainen P, Dasgupta J, Davidson JM, Wight TN, Helene Sage E. SPARC-null mice display abnormalities in the dermis characterized by decreased collagen fibril diameter and reduced tensile strength. J Invest Dermatol 120: 949-955, 2003.

Brandt T. Otolithic vertigo. Advances in Oto-Rhino-Laryngology 58: 34-47, 2001.

Brekken RA, Sage EH. SPARC, a matricellular protein: at the crossroads of cell-matrix. Matrix Biol 19: 569-580, 2000.

Campana SE, Thorrold SR. Otoliths, increments, and elements: keys to a comprehensive understanding of fish populations? Can J Fish Aquat Sci 58: 30-38, 2001.

Chu DT, Klymkowsky MW. The appearance of acetylated alpha-tubulin during early development and cellular differentiation in Xenopus. Dev Biol 136: 104-117, 1989.

Delany AM, Amling M, Priemel M, Howe C, Baron R, Canalis E. Osteopenia and decreased bone formation in osteonectin-deficient mice. J Clin Invest 105: 915-923, 2000.

Doi Y, Okuda R, Takezawa Y, Shibata S, Moriwaki Y, Wakamatsu N, Shimizu N, Moriyama K, Shimokawa H. Osteonectin inhibiting de novo formation of apatite in the presence of collagen. Calcif Tissue Int 44: 200-208, 1989.

Domon B, Aebersold R. Mass spectrometry and protein analysis. Science 312: 212-217, 2006.

Eckfeldt CE, Mendenhall EM, Flynn CM, Wang TF, Pickart MA, Grindle SM, Ekker SC, Verfaillie CM. Functional analysis of human hematopoietic stem cell gene expression using zebrafish. PLoS Biol 3: e254, 2005.

Fenyö D, Beavis RC. A method for assessing the statistical significance of mass spectrometry-based protein identifications using general scoring schemes. Anal Chem 75: 768-774, 2003.

Fisher LW, Hawkins GR, Tuross N, Termine JD. Purification and partial characterization of small proteoglycans I and II, bone sialoproteins I and II, and osteonectin from the mineral compartment of developing human bone. J Biol Chem 262: 9702-9708, 1987.

Gerwick L, Reynolds WS, Bayne CJ. A precerebellin-like protein is part of the acute phase response in rainbow trout, Oncorhynchus mykiss. Dev Comp Immunol 24: 597-607, 2000.

Gilmour DT, Lyon GJ, Carlton MB, Sanes JR, Cunningham JM, Anderson JR, Hogan BL, Evans MJ, Colledge WH. Mice deficient for the secreted glycoprotein SPARC/osteonectin/BM40 develop normally but show severe age-onset cataract formation and disruption of the lens. EMBO J 17: 1860-1870, 1998.

Gilmour DT, Jessen JR, Lin S. Manipulating gene expression in the zebrafish. In: Nüsslein-Volhard C and Dahm R (eds) Zebrafish. Oxford University Press, Oxford, pp. 121-143, 2002.

Gruber HE, Sage EH, Norton HJ, Funk S, Ingram J, Hanley EN, Jr. Targeted deletion of the SPARC gene accelerates disc degeneration in the aging mouse. J Histochem Cytochem 53: 1131-1138, 2005.

Haddon C, Lewis J. Early ear development in the embryo of the zebrafish, Danio rerio. J Comp Neurol 365: 113-128, 1996.

Hudspeth AJ. How the ear's works work. Nature 341: 397-404, 1989.

Hughes I, Thalmann I, Thalmann R, Ornitz DM. Mixing model systems: using zebrafish and mouse inner ear mutants and other organ systems to unravel the mystery of otoconial development. Brain Res 1091: 58-74, 2006.

Hunter GK, Hauschka PV, Poole AR, Rosenberg LC, Goldberg HA. Nucleation and inhibition of hydroxyapatite formation by mineralized tissue proteins. Biochem J 317 (Pt 1): 59-64, 1996.

Ingram RT, Clarke BL, Fisher LW, Fitzpatrick LA. Distribution of noncollagenous proteins in the matrix of adult human bone: evidence of anatomic and functional heterogeneity. J Bone Miner Res 8: 1019-1029, 1993.

Jowett T. Analysis of protein and gene expression. Methods Cell Biol 59: 63-85, 1999.

Kane DA, Kishimoto Y. Cell labelling and transplantation techniques. In: Nüsslein-Volhard C and Dahm R (eds) Zebrafish. Oxford University Press, Oxford, pp. 95-119, 2002.

Kappler JA, Starr CJ, Chan DK, Kollmar R, Hudspeth AJ. A nonsense mutation in the gene encoding a zebrafish myosin VI isoform causes defects in hair-cell mechanotransduction. Proc Natl Acad Sci U S A 101: 13056-13061, 2004.

Kawasaki K, Weiss KM. Evolutionary genetics of vertebrate tissue mineralization: the origin and evolution of the secretory calcium-binding phosphoprotein family. J Exp Zoolog B Mol Dev Evol 306: 295-316, 2006.

Kelm RJ, Jr., Swords NA, Orfeo T, Mann KG. Osteonectin in matrix remodeling. A plasminogen-osteonectin-collagen complex. J Biol Chem 269: 30147-30153, 1994.

Kimmel CB, Ballard WW, Kimmel SR, Ullmann B, Schilling TF. Stages of embryonic development of the zebrafish. Dev Dyn 203: 253-310, 1995.

Kollmar R, Fak J, Montgomery LG, Hudspeth AJ. Hair cell-specific splicing of mRNA for the alpha1D subunit of voltage-gated Ca2+ channels in the chicken's cochlea. Proc Natl Acad Sci U S A 94: 14889-14893, 1997.

Kollmar R, Nakamura SK, Kappler JA, Hudspeth AJ. Expression and phylogeny of claudins in vertebrate primordia. Proc Natl Acad Sci U S A 98: 10196-10201, 2001.

Korf I, Yandell M, Bedell J. BLAST. O'Reilly, Sebastopol, CA, 2003.

Kumar S, Hedges SB. A molecular timescale for vertebrate evolution. Nature 392: 917-920, 1998.

Kwan AP, Cummings CE, Chapman JA, Grant ME. Macromolecular organization of chicken type X collagen in vitro. J Cell Biol 114: 597-604, 1991.

Lopez R, Silventoinen V, Robinson S, Kibria A, Gish W. WU-Blast2 server at the European Bioinformatics Institute. Nucleic Acids Res 31: 3795-3798, 2003.

Lundberg YW, Zhao X, Yamoah EN. Assembly of the otoconia complex to the macular sensory epithelium of the vestibule. Brain Res 1091: 47-57, 2006.

Ma B, Zhang K, Hendrie C, Liang C, Li M, Doherty-Kirby A, Lajoie G. PEAKS: powerful software for peptide de novo sequencing by tandem mass spectrometry. Rapid Commun Mass Spectrom 17: 2337-2342, 2003.

Martinek N, Shahab J, Sodek J, Ringuette M. Is SPARC an evolutionarily conserved collagen chaperone? J Dent Res 86: 296-305, 2007.

Mei J, Gui J. Bioinformatic identification of genes encoding C1q-domain-containing proteins in zebrafish. J Genet Genomics 35: 17-24, 2008.

Miranda E, Lomas DA. Neuroserpin: a serpin to think about. Cell Mol Life Sci 63: 709-722, 2006.

Murayama E, Okuno A, Ohira T, Takagi Y, Nagasawa H. Molecular cloning and expression of an otolith matrix protein cDNA from the rainbow trout, Oncorhynchus mykiss. Comp Biochem Physiol B Biochem Mol Biol. 126: 511-520, 2000.

Murayama E, Takagi Y, Ohira T, Davis JG, Greene MI, Nagasawa H. Fish otolith contains a unique structural protein, otolin-1. Eur J Biochem. 269: 688-696, 2002.

Murayama E, Takagi Y, Nagasawa H. Immunohistochemical localization of two otolith matrix proteins in the otolith and inner ear of the rainbow trout, Oncorhynchus mykiss: comparative aspects between the adult inner ear and embryonic otocysts. Histochem Cell Biol 121: 155-166, 2004.

Murayama E, Herbomel P, Kawakami A, Takeda H, Nagasawa H. Otolith matrix proteins OMP-1 and Otolin-1 are necessary for normal otolith growth and their correct anchoring onto the sensory maculae. Mech Dev 122: 791-803, 2005.

Nemoto Y, Chatani M, Inohaya K, Hiraki Y, Kudo A. Expression of marker genes during otolith development in medaka. Gene Expr Patterns 8: 92-95, 2008.

Nolf D. Otolithi Piscium. Gustav Fischer, Stuttgart, 1985.

Pappin DJ, Hojrup P, Bleasby AJ. Rapid identification of proteins by peptide-mass fingerprinting. Curr Biol 3: 327-332, 1993.

Petko JA, Millimaki BB, Canfield VA, Riley BB, Levenson R. Otoc1: a novel otoconin-90 ortholog required for otolith mineralization in zebrafish. Dev Neurobiol 68: 209-222, 2008.

Piscopo M, Balsamo G, Mutone R, Avallone B, Marmo F. Calbindin D28K is a component of the organic matrix of lizard Podarcis sicula otoconia. Hear Res 178: 89-94, 2003.

Piscopo M, Avallone B, D'Angelo L, Fascio U, Balsamo G, Marmo F. Localization of calbindin D-28K in the otoconia of lizard Podarcis sicula. Hear Res 189: 76-82, 2004.

Pote KG, Hauer CR, 3rd, Michel H, Shabanowitz J, Hunt DF, Kretsinger RH. Otoconin-22, the major protein of aragonitic frog otoconia, is a homolog of phospholipase A2. Biochemistry 32: 5017-5024, 1993.

Puolakkainen P, Bradshaw AD, Kyriakides TR, Reed M, Brekken R, Wight T, Bornstein P, Ratner B, Sage EH. Compromised production of extracellular matrix in mice lacking secreted protein, acidic and rich in cysteine (SPARC) leads to a reduced foreign body reaction to implanted biomaterials. Am J Pathol 162: 627-635, 2003.

Renn J, Schaedel M, Volff JN, Goerlich R, Schartl M, Winkler C. Dynamic expression of sparc precedes formation of skeletal elements in the Medaka (Oryzias latipes). Gene 372: 208-218, 2006.

Rentz TJ, Poobalarahi F, Bornstein P, Sage EH, Bradshaw AD. SPARC regulates processing of procollagen I and collagen fibrillogenesis in dermal fibroblasts. J Biol Chem 282: 22062-22071, 2007.

Richardson KC, Jarett L, Finke EH. Embedding in epoxy resins for ultrathin sectioning in electron microscopy. Stain Technol 35: 313-323, 1960.

Riley BB, Zhu C, Janetopoulos C, Aufderheide KJ. A critical period of ear development controlled by distinct populations of ciliated cells in the zebrafish. Developmental Biology 191: 191-201, 1997.

Riley BB, Moorman SJ. Development of utricular otoliths, but not saccular otoliths, is necessary for vestibular function and survival in zebrafish. Journal of Neurobiology 43: 329-337, 2000.

Romberg RW, Werness PG, Riggs BL, Mann KG. Inhibition of hydroxyapatite crystal growth by bone-specific and other calcium-binding proteins. Biochemistry 25: 1176-1180, 1986.

Rotllant J, Liu D, Yan YL, Postlethwait JH, Westerfield M, Du SJ. Sparc (Osteonectin) functions in morphogenesis of the pharyngeal skeleton and inner ear. Matrix Biol, 2008.

Sage EH. Purification of SPARC/osteonectin. Curr Protoc Cell Biol Chapter 10: Unit 10.11, 2003.

Sakagami M. Role of osteopontin in the rodent inner ear as revealed by in situ hybridization. Med Electron Microsc 33: 3-10, 2000.

Secor DH, Dean JM, Laban EH. Manual for Otolith Removal and Preparation for Microstructural Examination. Electric Power Research Institute and the Belle W. Baruch Institute for Marine Biology and Coastal Research, 1991.

Shen G. The role of type X collagen in facilitating and regulating endochondral ossification of articular cartilage. Orthod Craniofac Res 8: 11-17, 2005.

Shevchenko A, Sunyaev S, Loboda A, Bork P, Ens W, Standing KG. Charting the proteomes of organisms with unsequenced genomes by MALDI-quadrupole time-of-flight mass spectrometry and BLAST homology searching. Anal Chem 73: 1917-1926, 2001.

Söllner C, Burghammer M, Busch-Nentwich E, Berger J, Schwarz H, Riekel C, Nicolson T. Control of crystal size and lattice formation by starmaker in otolith biomineralization. Science 302: 282-286, 2003.

Söllner C, Nicolson T. The Zebrafish as a Genetic Model to Study Otolith Formation. In: Bäuerlein E (ed) Biomineralization: Progress in Biology, Molecular Biology, and Application. Wiley-VCH, Weinheim, pp. 229-242, 2004.

Starr CJ, Kappler JA, Chan DK, Kollmar R, Hudspeth AJ. Mutation of the zebrafish choroideremia gene encoding Rab escort protein 1 devastates hair cells. Proc Natl Acad Sci U S A 101: 2572-2577, 2004.

Sumanas S, Larson JD, Miller Bever M. Zebrafish chaperone protein GP96 is required for otolith formation during ear development. Dev Biol 261: 443-455, 2003.

Sutmuller M, Bruijn JA, de Heer E. Collagen types VIII and X, two non-fibrillar, short-chain collagens. Structure homologies, functions and involvement in pathology. Histol Histopathol 12: 557-566, 1997.

Termine JD, Kleinman HK, Whitson SW, Conn KM, McGarvey ML, Martin GR. Osteonectin, a bone-specific protein linking mineral to collagen. Cell 26: 99-105, 1981.

Thalmann I, Hughes I, Tong BD, Ornitz DM, Thalmann R. Microscale analysis of proteins in inner ear tissues and fluids with emphasis on endolymphatic sac, otoconia, and organ of Corti. Electrophoresis 27: 1598-1608, 2006.

Thisse C, Thisse B. High-resolution in situ hybridization to whole-mount zebrafish embryos. Nat Protoc 3: 59-69, 2008.

Tohse H, Takagi Y, Nagasawa H. Identification of a novel matrix protein contained in a protein aggregate associated with collagen in fish otoliths. FEBS J 275: 2512-2523, 2008.

Tom Tang Y, Hu T, Arterburn M, Boyle B, Bright JM, Palencia S, Emtage PC, Funk WD. The complete complement of C1q-domain-containing proteins in Homo sapiens. Genomics 86: 100-111, 2005.

Varghese S. Matrix metalloproteinases and their inhibitors in bone: an overview of regulation and functions. Front Biosci 11: 2949-2966, 2006.

Verpy E, Leibovici M, Petit C. Characterization of otoconin-95, the major protein of murine otoconia, provides insights into the formation of these inner ear biominerals. Proc Natl Acad Sci U S A 96: 529-534, 1999.

Wang Y, Kowalski PE, Thalmann I, Ornitz DM, Mager DL, Thalmann R. Otoconin-90, the mammalian otoconial matrix protein, contains two domains of homology to secretory phospholipase A2. Proc Natl Acad Sci U S A 95: 15345-15350, 1998.

Weiner S, Addadi L. Design strategies in mineralized biological materials. J Mater Chem 7: 689-702, 1997.

Westerfield M. The zebrafish book: A guide for the laboratory use of zebrafish (Danio rerio). University of Oregon Press, Eugene, OR, 2000.

Whitfield TT, Riley BB, Chiang MY, Phillips B. Development of the zebrafish inner ear. Dev Dyn 223: 427-458, 2002.

Wittbrodt J, Shima A, Schartl M. Medaka—a model organism from the far East. Nat Rev Genet 3: 53-64, 2002.

Yaoi Y, Onda T, Hidaka Y, Yajima S, Suzuki M, Tanaka S. Developmental expression of otoconin-22 in the bullfrog endolymphatic sac and inner ear. J Histochem Cytochem 52: 663-670, 2004.

Zhang Z. Ultrastructure of otolith increments and checks in the teleost fish Oreochromis niloticus. J Morphol 211: 213-220, 1992.

Zhao X, Yang H, Yamoah EN, Lundberg YW. Gene targeting reveals the role of Oc90 as the essential organizer of the otoconial organic matrix. Dev Biol 304: 508-524, 2007.

Zhao X, Jones SM, Thoreson WB, Lundberg YW. Osteopontin is not Critical for Otoconia Formation or Balance Function. J Assoc Res Otolaryngol 9: 191-201, 2008.

Figure Legends

Fig. 1. Similarity and moderate complexity of protein complements in actinopterygian otoliths. (A) Otolith proteins of commercial and laboratory freshwater fishes separated by gel electrophoresis and stained with silver. Aliquots corresponding to about 1.2 mg otoliths per lane; apparent molecular masses in kDa indicated on the left. (B) Phylogeny of fish species mentioned in this study: White sturgeon *(Acipenser transmontanus),* zebrafish *(Danio rerio)*, bighead carp *(Aristichthys nobilis),* channel catfish *(Ictalurus punctatus),* black ghost *(Apteronotus albifrons),* rainbow trout *(Oncorhynchus mykiss),* chum salmon *(Oncorhynchus mykiss),* tilapia *(Oreochromis sp.),* japanese medaka *(Oryzias latipes),* torafugu *(Takifugu rubripes)*, spotted green pufferfish *(Tetraodon nigroviridis)*, and three-spined stickleback *(Gasterosteus aculeatus)*. Dotted lines in the cladogram indicate five or six actinopterygian clades each that were not represented. At three branch points, the estimated time since the last common ancestor is shown (Kumar and Hedges 1998; Wittbrodt et al. 2002).

Fig. 2. Localization of zebrafish Sparc mRNA in the ear and protein in otoliths. (A) The mRNAs of *sparc* and *β-actin* detected in whole embryos during early development by RT-PCR. (B-D) The mRNA of *sparc* detected in the developing ear by *in situ* hybridization. Dorsal views of hindbrain area, anterior at the top; outline in B, left otic placode; arrowheads in D, posterior maculae along the medial wall of the otic vesicle; arrows in D, semicircular canals; scale bar in B for all three panels, 50 μm. (E) Sparc protein detected in an adult-otolith extract by immunoblotting. About 0.6 μg total protein per membrane strip; Silver, silver-stained gel slice; Sparc, anti-Sparc serum UI-37; *E. coli*-adsorbed, UI-37 pre-adsorbed with a plain bacterial extract; Sparc-adsorbed, UI-37 pre-adsorbed with a bacterial extract containing recombinant

zebrafish Sparc; dashes on the right, molecular-mass markers (kDa, from top): 250, 160, 105, 75, 50, 35, 30, 25, 15, 10. (F) Sparc protein detected in otic vesicles by whole-mount immunofluorescence. Green, Sparc labeled with antiserum UI-37; blue, nuclei labeled with DAPI; arrowheads, lapillus (left) and sagitta (right); lateral view of otic vesicle, dorsal at the top, anterior to the left; projections of 10-μm stacks of optical sections; scale bar for panels F and G, 25 μm. (G) Same as F, but with purified naive rabbit IgG instead of UI-37. (H-I) Sparc protein detected in a transverse section of an adult lapillus. H, brightfield view of an otolith slice; I, immunofluorescence with antiserum UI-37 at the surface of the slice's cross-section; scale bar in H for panels H to M, 100 μm. (J-K) Same as H-I, but UI-37 pre-adsorbed with a plain bacterial extract. (L-M) Same as H-I, but UI-37 pre-adsorbed with a bacterial extract containing recombinant zebrafish Sparc. Because the brightfield images in H, J, and L were overexposed to visualize the growth rings, the visible otolith margins do not exactly match the fluorescent areas; I, K, and M are projections of 58 to 87-μm-thick stacks of optical sections that were acquired under matched settings.

Fig. 3. Diminished Sparc expression in morphant zebrafish embryos. (A) Schematic of the ATG-MO morpholino binding to the start codon of *sparc* mRNA and the e5i5-MO morpholino binding to the junction of exon 5 and intron 5. $GT_{a–c}$, splice donor sites; AG, splice acceptor site; For and Rev, PCR primers used in B. (B) Misspliced *sparc* mRNAs in e5i5-MO morphants at 28 hpf detected by RT-PCR. Injected reagents at the top; size markers in bp on the left; products derived from splicing at donor sites $GT_{a–c}$ or the unspliced pre-mRNA indicated on the right. (C) Example of protein detection in microinjected embryos at 52 hpf by two-color immunofluorescence blotting with antibodies against Sparc (red) and β-tubulin (green). Total

protein pooled from ten embryos each; equivalent of one embryo loaded per lane. (D) Summary of Sparc levels measured by immunofluorescence blotting. One set of injections each for ATG-MO and e5i5-MO; mean and range indicated by error bar for vehicle and Std-MO controls.

Fig. 4. Otolith abnormalities in zebrafish Sparc morphants. (A-D) Phenotypes of otoliths in microinjected embryos under brightfield illumination. Lateral views of otic vesicles, dorsal at the top, anterior to the left; arrowheads, lapillus (left) and sagitta (right) in A and extra/ectopic otolith in C; scale bar for all four panels in A, 30 μm; some ototliths were imaged in a slightly different focal plane. (E-I) Scanning electron micrographs of dissected otoliths from injected embryos. Scale bar for all five panels in E, 10 μm. (J-K) Structure of wild-type and morphant otoliths visualized by staining with toluidine blue. Coronal semi-thin sections of anterior maculae and lapilli; scale bar for both panels in K, 10 μm. (L) Summary of otolith areas measured in bright field images. Two-way ANOVA of three independent experiments for each morpholino; N = 94-107 per age and treatment for vehicle and Std-MO, 49-57 otherwise; error bars, 95% confidence intervals; *, significantly different in Bonferroni *post-hoc* pairwise comparisons from all other groups of the same age at $P \leq 10^{-4}$ and 403-418 df. (M-N) Hair bundles in wild-type and morphant anterior maculae visualized by labeling with fluorescent phalloidin. Dorsal views; projections of 17-μm stacks of optical sections; scale bar for both panels in N, 10 μm; 27 bundles in M, 26 in N. (O) Smaller otoliths in morphants regardless of otic-vesicle size. Only ears with both lapillus and sagitta, but no extra otoliths; r^2 of least-squares-fitted lines was 22%, 36%, and 39%, respectively, for Vehicle, ATG-MO, and e5i5-MO.

TABLE 1

Three proteins identified newly in otoliths by mass spectrometry[a]

Otolith Source	Top Database Match			Mascot Statistics			PEAKS/MS-BLAST Statistics		
	Species	GenBank Accession	Length (aa)	Nr of Peps	Covg	Expect[b]	Nr of Peps	Covg	Expect[c]
Secreted Protein, Acidic, Cysteine-Rich (Sparc)									
Trout	Trout	AAC99813.1	300	4	19%	$1.8 \cdot 10^{-9}$	5	22%	$7.3 \cdot 10^{-4}$
Catfish	Zebrafish	NP_001001942.1	291	2	11%	$3.2 \cdot 10^{-6}$	5	23%	$2.0 \cdot 10^{-3}$
”	Catfish[d]	ESTs CF262751.1 & CV987488.1	291	nd	nd	nd	5	23%	$1.2 \cdot 10^{-4}$
Precerebellin-Like Protein (Cblnl)									
Trout	Trout	AAF04305.2 (isoform a)	182	4	34%	$2.5 \cdot 10^{-7}$	4	32%	$1.3 \cdot 10^{-2}$
”	” [d]	ESTs CX140456.1 & CX140457.1 (isoform b)	206	nd	nd	nd	5	36%	$4.3 \cdot 10^{-4}$
Neuroserpin (Serpini1)									
Trout	Zebrafish	XP_685811.1	448	3	9%	$7.4 \cdot 10^{-4}$	–	–	–
”	Medaka	ENSORLP00000015491[e]	401	–	–	–	8	37%	$8.3 \cdot 10^{-4}$
”	Trout[d]	ESTs CA373728.1, CX251911.1, & CX251912.1	~416	nd	nd	nd	9	37%	$6.9 \cdot 10^{-8}$

[a] aa, amino acids; Pep, peptide; Covg, coverage; nd, not determined

[b] Based on the highest peptide MOWSE score

[c] Based on the protein BLAST *E*-value

[d] Identified in *post-hoc* BLAST search

[e] In Ensembl genome assembly HdrR

TABLE 2

Sparc, but not Sparcl identified in trout otoliths

Nr	*Origin*[a]	*Peptide*[b]
1	PEAKS	LHLDYLGPCK
	Sparc	K.LHLDYIGPCK.F
	Sparcl	R.LHLDYTGPCK.F
2	PEAKS	FLEACMDAELNEFPLR
	Sparc	K.FIEACMDAELNEFPLR.M
	Sparcl	K.FIAPCMNGELVQFPLR.M
3	PEAKS	NVLVSLYER
	Sparc	K.NVLVTLYER.D
	Sparcl	K.NVLLQLYEH.D
4	PEAKS	LQAGEHSLDLLAHDFEK
	Sparc	R.LQAGEHSLDLLAHDFEK.N
	Sparcl	R.LHAGDHPIELLAQDFEK.D
5	PEAKS	LYALEEWANCFSLK
	Sparc	K.YIALEEWANCFSIK.E
	Sparcl	[EST too short at 3' end]

[a]PEAKS, prediction from mass spectrum; bold, mass error <0.03; Sparcl accession, BX909167.3.

[b]Mismatches with PEAKS shaded (I & L treated as identical); flanking residues separated by '.'.

TABLE 3

Two Cblnl isoforms identified in trout otoliths[a]

Nr	*Origin*	*Peptide*[b]
1	PEAKS	ESEVDGLLR
	Cblnl-a	T-ESEVDGLLR.E
	Cblnl-b	T-ESEVDGLLR.E
2	PEAKS	VSDEHYHLGPFDK
	Cblnl-a	M.INDEHYHLGPFGE.N
	Cblnl-b	R.VSDEHYHLGPFDK.Y
3	PEAKS	VLTNLGEAYNPDTGVFTAPVR
	Cblnl-a	K.VITNIGEAYNPDTGVFTAPVR.G
	Cblnl-b	K.VTTNIGEAYNPDTGVFTAPVR.G
4	PEAKS	SGLYHE-VAGVTLDLVK
	Cblnl-a	K.SGIYHGGANGVTLDLVK.G
	Cblnl-b	K.SGVYHSGANGVTLDLVE.G
5	PEAKS	LSMFSGYLLFPLDNK
	Cblnl-a	R.INMFSGYLLFPITTK.*
	Cblnl-b	R.ISMFSGYLLFPIDNK.*

[a]Key, see Table 2; Cblnl accessions, see Table 1.

[b]–, signal-peptide cleavage site; *, C-terminus.

TABLE 4

Retention of Lapillus and Sagitta in Sparc morphants

Treatment	*Percentage of Embryos with Otoliths Present*[a]			
	Lap. & Sag.	*Lap.*	*Sag.*	*Neither*
28 hpf				
Vehicle	97 / 3	– / –	– / –	– / –
Std-MO	88 / 11	– / –	– / –	1 / –
ATG-MO	56 / 29	– / 2	4 / –	9 / –
ATGmis-MO	85 / 15	– / –	– / –	– / –
e5i5-MO	53 / 27	2 / –	– / –	18 / –
e5i5mis-MO	78 / 20	– / –	– / –	2 / –
52 hpf				
Vehicle	100 / –	– / –	– / –	– / –
Std-MO	100 / –	– / –	– / –	– / –
ATG-MO	76 / 13	4 / –	4 / –	4 / –
ATGmis-MO	100 / –	– / –	– / –	– / –
e5i5-MO	50 / 46	4 / –	– / –	– / –
e5i5mis-MO	94 / 6	– / –	– / –	– / –
76 hpf				
Vehicle	99 / 1	– / –	– / –	– / –
Std-MO	99 / –	– / –	– / –	1 / –
ATG-MO	72 / 12	2 / –	9 / 2	2 / 2
ATGmis-MO	100 / –	– / –	– / –	– / –
e5i5-MO	68 / 21	2 / 2	5 / –	2 / –
e5i5mis-MO	100 / –	– / –	– / –	– / –

[a]Without any extra otoliths / with 1-3 extra otoliths; *e.g.,* first row, first column: 97% with lapillus (Lap.) and sagitta (Sag.) alone / 3% with lapillus and sagitta plus extra otoliths; *N* = 94-107 per age for Vehicle & Std-MO, 49-57 otherwise.

TABLE 5

Milder otic-vesicle phenotype in e5i5-morphants

Treatment	*Otic-vesicle area ($10^3 \cdot \mu m^2$)*[a]		
52 hpf			
Vehicle	8.17 ± 0.14	(100)	
Std-MO	8.16 ± 0.13	(102)	
ATG-MO	5.92 ± 0.18	(55)	**
ATGmis-MO	7.29 ± 0.19	(52)	*
e5i5-MO	8.26 ± 0.19	(51)	
e5i5mis-MO	8.26 ± 0.19	(53)	
76 hpf			
Vehicle	14.72 ± 0.30	(94)	
Std-MO	14.52 ± 0.28	(107)	
ATG-MO	11.40 ± 0.31	(55)	**
ATGmis-MO	13.15 ± 0.35	(55)	*
e5i5-MO	14.93 ± 0.40	(55)	
e5i5mis-MO	13.90 ± 0.39	(49)	

[a]Mean ± SEM *(n)*

*Significantly different from 'Vehicle' *($P \leq 0.01$)*

**Significantly different from 'Vehicle' *($P < 10^{-4}$)*

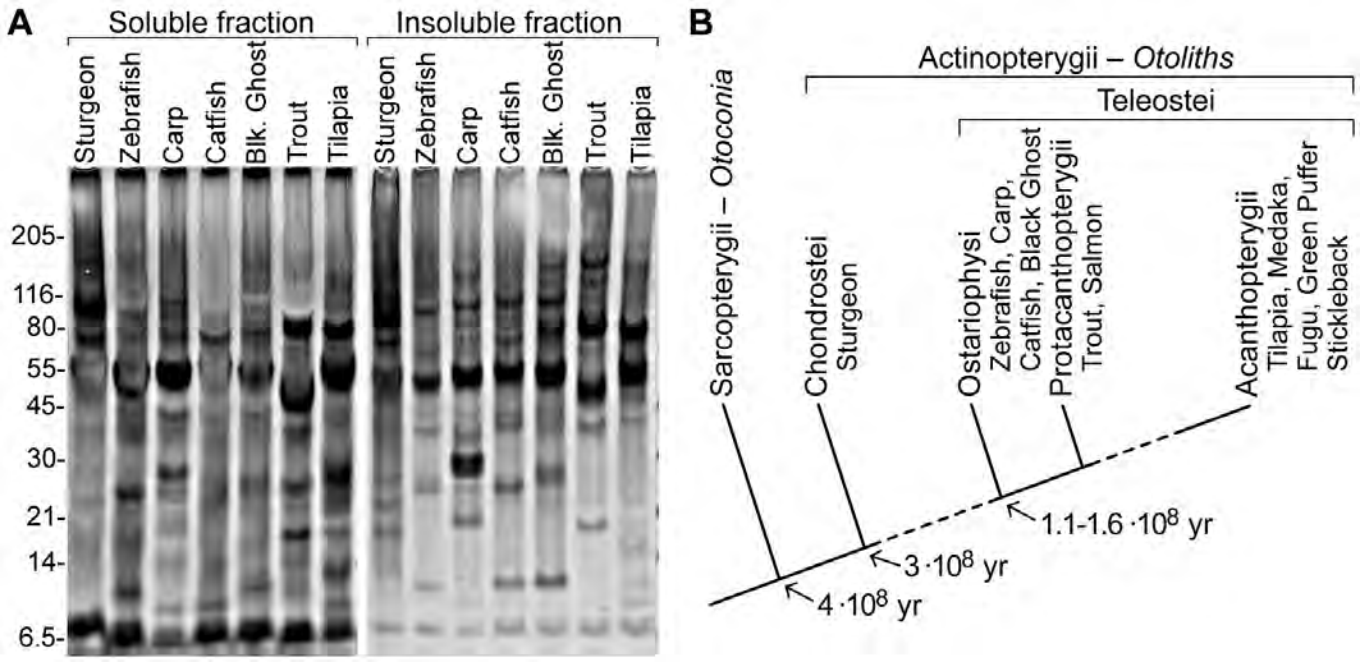
A
Soluble fraction
Insoluble fraction
Sturgeon
Zebrafish
Carp
Catfish
Blk. Ghost
Trout
Tilapia
205-
116-
80-
55-
45-
30-
21-
14-
6.5-
B
Actinopterygii – Otoliths
Teleostei
Sarcopterygii – Otoconia
Chondrostei
Sturgeon
Ostariophysi
Zebrafish, Carp,
Catfish, Black Ghost
Protacanthopterygii
Trout, Salmon
Acanthopterygii
Tilapia, Medaka,
Fugu, Green Puffer
Stickleback
1.1-1.6 ·10^8 yr
3 ·10^8 yr
4 ·10^8 yr

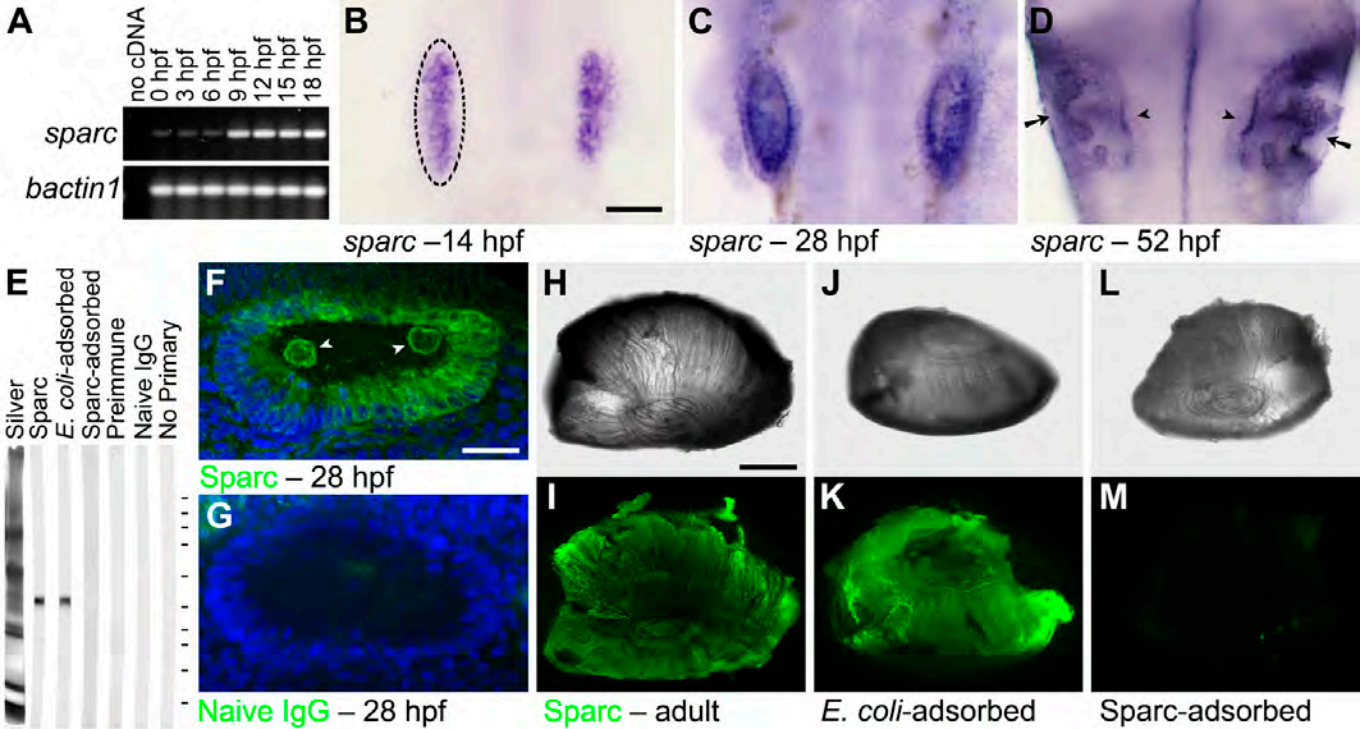
A
no cDNA
0 hpf
3 hpf
6 hpf
9 hpf
12 hpf
15 hpf
18 hpf
sparc
bactin1
B
C
D
sparc –14 hpf
sparc – 28 hpf
sparc – 52 hpf
E
Silver
Sparc
E. coli-adsorbed
Sparc-adsorbed
Preimmune
Naive IgG
No Primary
F
Sparc – 28 hpf
G
Naive IgG – 28 hpf
H
I
Sparc – adult
J
K
E. coli-adsorbed
L
M
Sparc-adsorbed

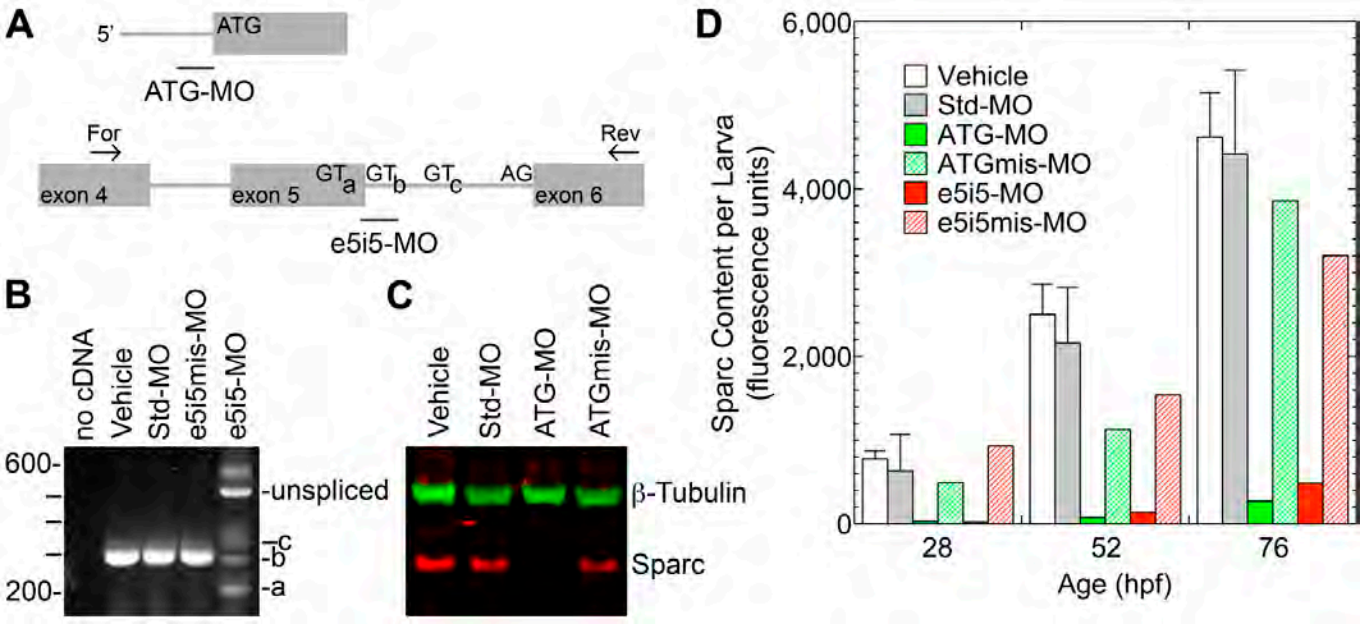
A
5'
ATG
ATG-MO
For
Rev
exon 4
exon 5
GTa
GTb
GTc
AG
exon 6
e5i5-MO
B
no cDNA
Vehicle
Std-MO
e5i5mis-MO
e5i5-MO
600-
200-
-unspliced
-b
-c
-a
C
Vehicle
Std-MO
ATG-MO
ATGmis-MO
β-Tubulin
Sparc
D
Vehicle
Std-MO
ATG-MO
ATGmis-MO
e5i5-MO
e5i5mis-MO
Sparc Content per Larva
(fluorescence units)
6,000
4,000
2,000
0
28
52
76
Age (hpf)

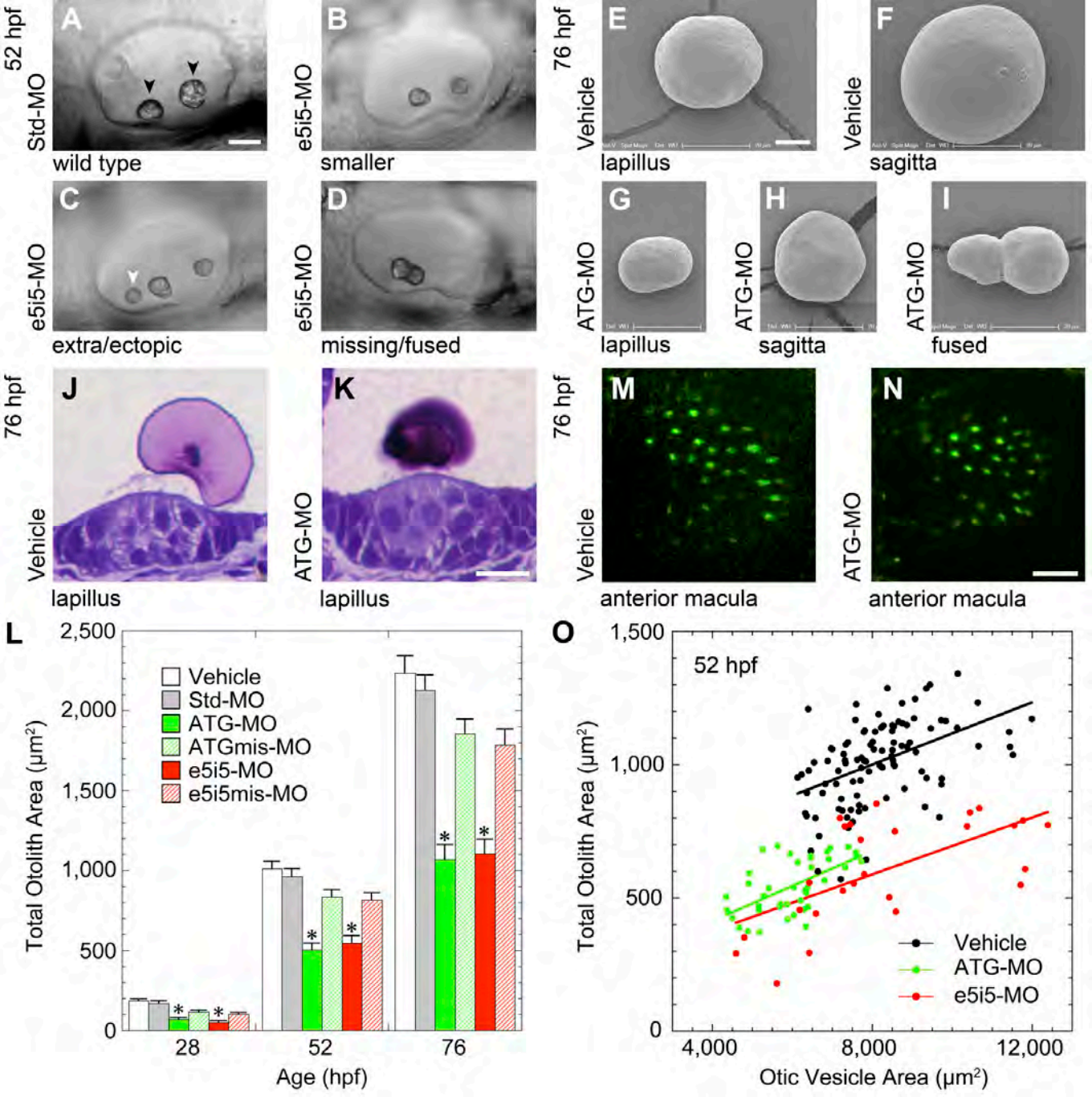
52 hpf
Std-MO
A
wild type
B
e5i5-MO
smaller
C
e5i5-MO
extra/ectopic
D
e5i5-MO
missing/fused
76 hpf
Vehicle
E
lapillus
F
Vehicle
sagitta
G
ATG-MO
lapillus
H
ATG-MO
sagitta
I
ATG-MO
fused
76 hpf
Vehicle
J
lapillus
K
ATG-MO
lapillus
76 hpf
Vehicle
M
anterior macula
N
ATG-MO
anterior macula
L
Total Otolith Area (μm²)
2,500
2,000
1,500
1,000
500
0
Vehicle
Std-MO
ATG-MO
ATGmis-MO
e5i5-MO
e5i5mis-MO
28
52
76
Age (hpf)
O
52 hpf
Total Otolith Area (μm²)
1,500
1,000
500
0
Vehicle
ATG-MO
e5i5-MO
4,000
8,000
12,000
Otic Vesicle Area (μm²)